AD-A173 130 RED SOX (SINGLET OXYGEN) LASER: A CHEMICALLY-PUMPED 076 1/1
MICROMETERS SINGL..(U) KMS FUSION INC ANN ARBOR MI
G E BUSCH ET AL. 28 FEB 86 AFOSR-TR-86-0961
UNCLASSIFIED F49620-85-C-0104 F/G 20/5 NL

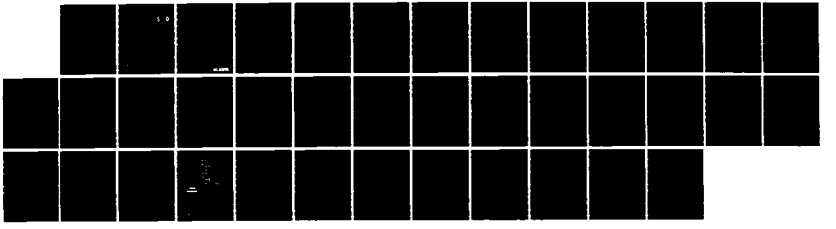

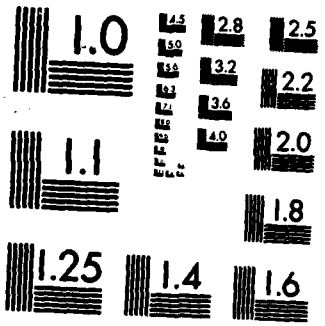

MICROCOPY RESOLUTION TEST CHART
NATIONAL BUREAU OF STANDARDS-1963-A

AFOSR-TR- 86-0961

Final Report

Phase I SBIR
Contract #F49620-85-C-0104

Red SOX Laser: A Chemically-Pumped, 0.76 μm Singlet Oxygen Laser

George E. Busch
and
Mark B. Knickelbein
KMS Fusion, Inc.
3621 S. State Rd.
Ann Arbor, MI 48106

28 February 1986

Prepared for
Air Force Office of Scientific Research
Building 410, Room A113
Bolling Air Force Base
Washington, D.C. 20332-6448

UNCLASSIFIED
SECURITY CLASSIFICATION OF THIS PAGE

AD-A173130

REPORT DOCUMENTATION PAGE

1a. REPORT SECURITY CLASSIFICATION UNCLASSIFIED	1b. RESTRICTIVE MARKINGS
2a. SECURITY CLASSIFICATION AUTHORITY	3. DISTRIBUTION/AVAILABILITY OF REPORT Approved for public release, distribution unlimited
2b. DECLASSIFICATION/DOWNGRADING SCHEDULE	
4. PERFORMING ORGANIZATION REPORT NUMBER(S)	5. MONITORING ORGANIZATION REPORT NUMBER(S) AFOSR-TR- 86-0961
6a. NAME OF PERFORMING ORGANIZATION KMS FUSION, INC. — 6b. OFFICE SYMBOL (If applicable)	7a. NAME OF MONITORING ORGANIZATION AFOSR
6c. ADDRESS (City, State and ZIP Code) 3621 S. State Rd. Ann Arbor, MI 48106	7b. ADDRESS (City, State and ZIP Code) AFOSR/NP, Bldg 410 Bolling AFB, DC 20332-6448
8a. NAME OF FUNDING/SPONSORING ORGANIZATION AFOSR — 8b. OFFICE SYMBOL (If applicable) NP	9. PROCUREMENT INSTRUMENT IDENTIFICATION NUMBER F49620-85-C-0104
8c. ADDRESS (City, State and ZIP Code) AFOSR/NP, Bldg 410 Bolling AFB, DC 20332-6448	10. SOURCE OF FUNDING NOS. PROGRAM ELEMENT NO.: 61102F — PROJECT NO.: 2301 — TASK NO.: A1 — WORK UNIT NO.: N/A
11. TITLE (Include Security Classification) "RED SOX LASER: A CHEMICALLY PUMPED, 0.76 um SINGLET OXYGEN LASER"	
12. PERSONAL AUTHOR(S) Dr. George E. Busch	
13a. TYPE OF REPORT FINAL — 13b. TIME COVERED FROM 85/07/01 TO 85/12/31	14. DATE OF REPORT (Yr., Mo., Day) 28 Feb 86 — 15. PAGE COUNT 33
16. SUPPLEMENTARY NOTATION	
17. COSATI CODES FIELD / GROUP / SUB. GR.	18. SUBJECT TERMS (Continue on reverse if necessary and identify by block number)

19. ABSTRACT (Continue on reverse if necessary and identify by block number)

The feasibility of a red singlet oxygen laser based ib production of (b) state singlet oxygen by the electronic energy pooling reaction of (a) state singlet oxygen was investigated. A microwave discharge-flow system for studying the quenching kinetics of (b) state oxygen was constructed with a large diameter viewing region so as to ensure that heterogeneous quenching of both (a) and (b) state oxygen was unimportant. An upper bound for quenching of (b) state oxygen by (a) state oxygen was measured and was not found to be extremely large compared to the rate constant for quenching of (b) state oxygen by ground state oxygen.

20. DISTRIBUTION/AVAILABILITY OF ABSTRACT UNCLASSIFIED/UNLIMITED ☒ SAME AS RPT. ☒ DTIC USERS ☐	21. ABSTRACT SECURITY CLASSIFICATION UNCLASSIFIED
22a. NAME OF RESPONSIBLE INDIVIDUAL HOWARD R. SCHLOSSBERG	22b. TELEPHONE NUMBER (Include Area Code) 202/767-4906 — 22c. OFFICE SYMBOL NP

DD FORM 1473, 83 APR — EDITION OF 1 JAN 73 IS OBSOLETE.

UNCLASSIFIED

Abstract

The feasibility of a red singlet oxygen laser based on production of (b) state singlet oxygen by the electronic energy pooling reaction of (a) state singlet oxygen was investigated. A microwave discharge-flow system for studying the quenching kinetics of (b) state obygen was constructed with a large diameter viewing region so as to ensure that heterogeneous quenching of both (a) and (b) state oxygen was unimportant.

An upper bound for quenching of (b) state oxygen by (a) state oxygen was measured and was not found to be extremely large compared to the rate constant for quenching of (b) state oxygen by ground state oxygen.

The rate constants for quenching of both (b) state oxygen and (a) state oxygen by ground state oxygen was measured. Both rate constants agreed well with those measured by previous workers.

The results suggest that the extent of the effective population inversion of (b) state oxygen produced energy pooling will not be suppressed by the high densities of (a) state oxygen initially present. The measurements reported here support the feasibility of the red singlet oxygen (Red SOX) laser and further research and development toward this goal is recommended.

Table of Contents

A. Introduction

Chemical lasers are among the devices being considered for delivery of high-power directed energy. The high energy storage density potentially available with chemicals makes chemical lasers particularly attractive for airborne missions, where weight considerations are important. However, chemical systems presently under evaluation suffer from a number of drawbacks which are expected to be greatly reduced in the Singlet Oxygen (SOX) laser which is the subject of this proposal.

Chemical lasers fall into two principal groups, depending on whether the spectroscopic transition involves vibrational excitation of a molecule or electronic excitation of an atom or molecule. Examples of the former laser group are the HF and DF lasers, pumped by reacting fluorine or a fluorine-containing compound with H_2 or D_2. These lasers are plagued with problems of fluid dynamics associated with high energy release, extremely rapid rates for reaction, and comparatively fast collisional deactivation rates. In addition, the long wavelengths (2.4 - 3.8 μm) present problems of atmospheric transmission and low brightness, the latter of which scales with λ^{-2}.

The only known example of a scalable electronic transition laser is the chemical oxygen-iodine laser (COIL),[1-3] in which electronic excitation of metastable $O_2(^1\Delta)$ molecules, produced by chemical reaction of chlorine with basic hydrogen peroxide, is transferred to atomic iodine. The laser operated on the iodine transition at 1.3 μm. While the wavelength of the COIL laser permits over eight times the brightness of a DF laser operating at the same power level, frequency doubling and tripling are still being considered to further improve brightness. Other important issues in COIL are: the need for supersonic flows to improve medium homogeneity and counteract high quenching rates, the uncertainty about the mechanism of I_2 dissociation and thus the

scalability to higher densities, problems in obtaining uniform mixing on a short time-scale, and the need for generators of $O_2(^1\Delta)$ that will operate at low gravity and variable acceleration.

There is thus an impetus to look for new chemical lasers that might have shorter wavelengths and fewer fluid dynamic and kinetic rate limitations than current systems under consideration. A laser based on conversion of chemically-produced $O_2(^1\Delta)$ to $O_2(^1\Sigma)$ is proposed as a viable candidate. The lasing wavelength of 0.76 μm could provide three times the brightness of a COIL laser. The expected slowness of quenching reactions as well as primary production would greatly reduce hydrodynamic and kinetic mixing constraints and provide for large, uniform gain regions.

In the past,[4,5] attempts have been made to obtain direct lasing of $O_2(^1\Delta)$, motivated by a desire to circumvent complications that arise from mixing of iodine in a COIL laser. These attempts have been unsuccessful because of the low cross-section for stimulated emission and thus, low gain of an $O_2(^1\Delta)$ laser. This difficulty could be greatly reduced in a laser utilizing $O_2(^1\Sigma)$

$$O_2(^1\Sigma) \rightarrow O_2(^3\Sigma) + h\nu$$

because the cross-section, and thus the small signal gain coefficient for the Doppler-broadened transition, is over 50 times greater than for the transition in $O_2(^1\Delta)$.

The source of $O_2(^1\Sigma)$ for a laser would probably be the energy pooling reaction

$$2\ O_2\ (\tilde{a}\ ^1\Delta_g) \xrightarrow{k_p} O_2\ (b\ ^1\Sigma_g^+) + O_2\ (X\ ^3\Sigma_u^-) \qquad (1)$$

As set forth in the Phase I Statement of Work, the primary goal of this investigation has been to measure the rate constant for quenching of $O_2(^1\Sigma)$ by O_2 $(^1\Delta)$:

$$O_2\ (^1\Sigma) + O_2\ (^1\Delta) \xrightarrow{k_{\Sigma 2a}} O_2\ (^1\Delta) + O_2(^1\Delta) \qquad (2a)$$

$$\xrightarrow{k_{\Sigma 2b}} O_2\ (^1\Delta) + O_2(^3\Sigma) \qquad (2b)$$

Reactions (2a) and (2b) are potentially important sources of deactivation of $O_2(^1\Sigma)$ under the initial conditions of high $O_2(^1\Delta)$ density. The production of an electronic population inversion in O_2 requires that (2a) and (2b) be slow reactions relative to Reaction (1). The aim of Phase I of this project has been to quantitatively assess the importance of Reactions (2a) and (2b) in gaseous oxygen systems by obtaining an estimate to $k_{\Sigma 2}$.

We next discuss the results of our Phase I investigation and their significance to the Phase II effort. In Section B we will discuss the experimental apparatus and procedures used to perform the measurements. In Section C we give a kinetic analysis for the steady state and time dependent density of $O_2(^1\Delta)$ and $O_2(^1\Sigma)$. The experimental results are presented and discussed in Section D.

B. Experimental Apparatus and Procedures

The measurements have been performed using a discharge flow apparatus with a large (60 cm) diameter viewing region, a schematic of which is shown in Figure 1. Flow rates were measured using a calibrated mass flow meter (Scott) and pressure was measured to within 0.02 Torr by a capacitance manometer (FPI).

Singlet oxygen was produced by a 2.45 GHz microwave discharge through four parallel 3.9 cm i.d. quartz tubes. Surrounding each quartz tube was a microwave cavity containing three magnetrons (Toshiba 2M205 and 2M207) driven by a 208 V three phase circuit such that each magnetron within a group was driven 120° out of phase with respect to the other two. By monitoring the O_2 ($^1\Delta$) and O_2 ($^1\Sigma$) density downstream of the discharge we were able to verify that this discharge arrangement produced steady densities of $O_2(^1\Delta)$ and $O_2(^1\Sigma)$ with no evidence of modulation at 60 Hz.

The density of $O_2(^1\Delta)$ was measured with a germanium photodiode (Judson J-16D) cooled to 77 K and calibrated against a standard tungsten lamp. An interference filter with approximately 90 nm bandpass isolated the 1.27 μ ($\tilde{a} \rightarrow \tilde{X}$) fundamental emission of $O_2(^1\Delta)$. The current output of the photodiode was measured using a Keithley 410A picoammeter.

Both detectors were mounted on carriers which moved along an optical rail parallel to the vessel axis. The O_2 ($^1\Sigma$) density was measured with a Hamamatsu R1104 photomultiplier tube calibrated against the same standard lamp and equipped with a 5.5 nm bandpass interference filter centered at 760 nm which isolated the $\tilde{b} \rightarrow \tilde{X}$ transition. The PMT signal was observed on an oscilloscope with 1.00 MΩ input impedance. Each detector was equipped with imaging optics so that the center of the viewing vessel and the detector faces were conjugate points. This arrangement provided for uniform weighting of densities at each radial position in the vessel, i.e. the detected signal S_i for species i is given by

$$S_i = C_i \int_{-R}^{R} \rho_i(r)dr \qquad (3)$$

in which $\rho_i(r)$ is the density of species i and C_i is a calibration factor

relating density of species i to signal strength. R is the tube radius. Note however, that if $\rho_i(r)$ constant, then Equation (3) does not properly weight the density $\rho_i(r)$ to give a signal proportional to the average density over the tube cross-section. The latter would require an additional factor of r under the integral in order to weight regions near the vessel wall

$$S_i' = C_i' \int_0^R r\rho_i(r)dr \ . \qquad (4)$$

For parabolic distributions of the type $\rho(r) = \rho_o(r^2 + \text{const})$ or $\rho(r) = \rho_o(R^2-r^2)$, which are expected when species are produced or destroyed at the wall, the difference between Equations (3) and Eq. (4) can be large. Measurements were made to determine whether densities were strongly dependent on r, and these measurements will be reported in Section 3D.

Impurities

For the present investigation it was important to verify that quenching of $O_2(^1\Delta)$ and $O_2(^1\Sigma)$ by species other than O_2 was not important. The species which posed the greatest potential for complicating our quenching kinetics results were NO_2, O_3, O, and H_2O. Bimolecular rate constants for quenching and other reactions involving $O_2(^1\Delta)$ and $O_2(^1\Sigma)$ are given in Table 1. We have evaluated the effects of these species as follows.

NO_2. Nitrogen dioxide is formed in oxygen discharges when N_2 is present as an impurity in commercial oxygen. NO_2 is a known quencher of $O_2(^1\Delta)$ and $O_2(^1\Sigma)$, with quenching rate constants of 5×10^{-18} and 2×10^{-14} cm^3 $molec^{-1}$ sec^{-1}, respectively (See Table 1). Assuming the extreme case that all of the N_2 present in a 1 Torr flow of oxygen (< 10 p.p.m.) is converted to NO_2, the pseudo-first order rate constants for quenching $O_2(^1\Delta)$ and $O_2(^1\Sigma)$ are 6.4×10^{-6}

and 3.2×10^{-2} sec^{-1}, respectively. The corresponding pseudo-first order rate constants for quenching of $O_2(^1\Delta)$ and $O_2(^1\Sigma)$ by ground state oxygen at 1 Torr are 5×10^{-2} and 1.4 sec^{-1}, respectively. We conclude that quenching by NO_2 is not significant in this experiment.

O_3,O. In low pressure oxygen discharges, oxygen atoms, molecular oxygen and ozone participate in a coupled kinetic scheme. The rate constants for quenching of $O_2(^1\Delta)$ and $O_2(^1\Sigma)$ by O_3 and O are given in Table 1. The dominant homogeneous reactions occurring downstream of the discharge governing the production and destruction of these species can be summarized by the following kinetic scheme.

$$O + O_2 + O_2 \xrightarrow{k_5} O_3 + O_2 \tag{5}$$

$$O_3 + O_2\,(^1\Delta) \xrightarrow{k_6} O + O_2 + O_2 \tag{6}$$

$$O_3 + O \xrightarrow{k_7} O_2 + O_2 \tag{7}$$

The rate equations describing the disappearance of O and O_3 are

$$\frac{-d[O_3]}{dt} = -k_5\,[O]\,[O_2]^2 + k_6\,[O_3][O_2{}^1\Delta] + k_7[O_3][O] \tag{8}$$

$$\frac{-d[O]}{dt} = k_5[O][O_2]^2 - k_6\,[O_3][O_2{}^1\Delta] + k_7\,[O_3][O] \tag{9}$$

Since O_2 $(^3\Sigma)$ and O_2 $(^1\Delta)$ are the dominant species present in the discharge, Equations (8) and (9) may be rewritten in pseudo-first order form

$$\frac{-d[O_3]}{dt} = -k_5'\,[O] + k_6'\,[O_3] + k_7\,[O_3][O] \tag{10}$$

$$\frac{-d\,[O]}{dt} = k_5' [O] - k_6' [O_3] + k_7 [O_3][O] \qquad (11)$$

where $k_5' = k_5 [O_2]^2$ and $k_6' = k_6 [O_2\,^1\Delta]$. Using the literature values (Table 1) for k_5 and k_6, and using typical values for O_2 and $O_2(^1\Delta)$ of 1 Torr and 0.1 Torr respectively, we find that $k_5' \cong 0.4\ sec^{-1}$ and $k_6' \cong 11\ sec^{-1}$.

Reactions (5) and (6) do not result in net removal of O_3 and O. In the gas phase removal is governed by Reaction (7), that is, the direct reaction of O_3 and O, with $k_7 = 6.2 \times 10^{-15}\ cm^3\ molec^{-1}\ sec^{-1}$. Assuming equal initial densities of O_3 and O (say $10^{14}\ cm^{-3}$) the decay will be second order with the first half life $(k_7[O])^{-1} = 1.6$ sec. The decay times of $O_2(^1\Delta)$ and $O_2(^1\Sigma)$ are comparable to or shorter than this at O_3 and concentration of $10^{14}\ cm^{-3}$. We conclude that gas phase reactions will not quantitatively remove O_3 or oxygen atoms sufficiently rapidly to prevent their quenching of $O_2(^1\Delta)$ and $O_2(^1\Sigma)$.

In addition to removal of O_3 and O by homogeneous reaction, oxygen atoms recombine on the walls of the discharge tube.[32] Formation of a post-discharge HgO film on the inner surfaces of the quartz tubes by addition of Hg to the O_2 flow prior to discharge is known[7,24,26] to increase the rate of O atom recombination. During the course of this study the effect of operating the discharge with and without the HgO film was investigated. It was found that with the HgO film in place, the steady state density of $O_2(^1\Delta)$ was not significantly different from that measured with no film, however the density of $O_2(^1\Sigma)$ was an order of magnitude larger. Given the large rate constants for quenching of $O_2(^1\Sigma)$ by O_3 and O we conclude that the HgO film probably significantly reduces O_3 and O density, but the evidence is indirect, and we did not have the capability to establish the presence of these species nor to determine whether removal of these species is nearly complete in the presence of the HgO film.

H_2O. The rate constant for quenching of $O_2(^1\Sigma)$ by H_2O is 6×10^{-12} cm^3 $molec^{-1}$ sec^{-1} (see Table 1). For this reason we have taken care to exclude traces of water from the flow system by passing O_2 through a stainless steel coil, 200 cm in length submersed in liquid nitrogen upstream to the discharge apparatus. The complete apparatus was purged for at least 12 hours prior to operation with a slow flow of 99.993% O_2 (< 10 p.p.m. H_2O). We estimate residual H_2O density from inboard leaks to be less than 1 p.p.m. at all flow rates used, based on leak rate and humidity, but quantitative measurements should be made in the Phase II experiments.

Heterogeneous Quenching of $O_2(^1\Sigma)$ and $O_2(^1\Delta)$

It has been previously established[23] that $O_2(^1\Sigma)$ quenches on Pyrex glass surfaces with a quenching efficiency, γ, of 10^{-2} - 10^{-3}. The effective rate constant for quenching of an excited species flowing in a tube of cylindrical cross section of radius r is given by:

$$k_{HE} = \left(\frac{r^2 P}{8D_o} + \frac{2r}{\gamma \bar{u}}\right)^{-1} \qquad (12)$$

Where P, D_o and $\bar{u}$ represent the overall pressure, the diffusion coefficient and the mean molecular speed, respectively. The relative contribution of each term in k_{HE} is summarized in Table 2 for several total pressures in the range 0.1 - 10 Torr. For $O_2(^1\Delta)$ at all pressures, the second term in Equation 2 dominates and hence the actual process of heterogeneous quenching at the wall is the rate limiting step. Using the values in Table 2, $k_{HE} < 0.01$ sec^{-1} so that the heterogeneous quenching lifetime is greater than 100 sec. Since the transit time of a given volume element through the observation vessel ranged from 2 to 20 seconds, the depletion of $O_2(^1\Delta)$ by heterogeneous quenching is

clearly negligible in the present experiments.

For $O_2(^1\Sigma)$, heterogeneous quenching passes through two regimes, changing from quenching rate limited at 0.1 Torr to diffusion rate limited at 10 Torr. The present experiments were performed in the 1-4 Torr range, where heterogeneous quenching is neither strictly diffusion controlled nor quenching rate controlled. At 1.0 Torr $k_{HE} \cong 0.8$ sec^{-1}, giving an effective lifetime of ~ 1.3 seconds in the vessel. At 1 Torr the pseudo-first order homogeneous rate constant for quenching of $O_2(^1\Sigma)$ by ground state O_2 is 1.3 sec^{-1}. At 4 Torr $k_{HE} \cong 0.2$ sec^{-1} while the rate constant for quenching by ground state increases to 5.2 sec^{-1}. With a transit time of 2 to 20 seconds in the vessel, heterogeneous quenching of $O_2(^1\Sigma)$ is clearly important at pressures of ~ 1 Torr while at 4 Torr homogeneous quenching dominates. In the limit where wall quenching is diffusion controlled, the density profile of $O_2(^1\Sigma)$ within the tube is expected to be parabolic, with maximum density in the tube center and zero density at the wall. We have measured $O_2(^1\Sigma)$ density at different distances from the center line in the observation vessel, taking into account the diminishing volume viewed as the detector is moved toward the edge of the tank. The results, shown in Figures 2-4 show that at P = 0.4 and 0.8 Torr there is no clearcut evidence of a $O_2(^1\Sigma)$ density gradient between the tube center and the wall. Nevertheless, wall quenching of $O_2(^1\Sigma)$ is expected to be important as pressures approach 1 Torr. The results could be explained if $\gamma << 2.5 \times 10^{-3}$ in Equation (12).

Flow System Characteristics

The time base used for the monitoring of $O_2(^1\Delta)$ and $O_2(^1\Sigma)$ concentrations is determined by the linear flow speed of O_2 in the observation vessel and the distance downstream in the direction of flow. This simple method for defining

the time evaluation of the composition of a given volume element of gas is strictly rigorous only in the case of "plug" flow where the diffusion rate in the direction of flow is much smaller than the linear flow rate.

For the present system, we have attempted to initially create plug-like flow in the observation chamber by installation of polycarbonate honeycomb flow straighteners covered on one side with 80 micron Teflon screen (see Figure 1). To observe the effect of these devices on flow characteristics we rendered the flow visible by the addition of N_2 to the O_2 flow upstream of the discharge. The ensuing NO_2 glow is long lived and easily visible with the room darkened. We were able to determine qualitatively that the flow straighteners effectively reduced the kinetic energy of the gas flow from the 2" lead-in pipes, converting dynamic pressure to static pressure. The NO_2 glow uniformly filled the bell shaped reducer leading into the observation chamber. The second baffle was designed to further reduce the flow kinetic energy.

Without the baffles, we observed turbulent streaming of the NO_2 glow into the center of the tank, with stagnation occurring at the tank edges. Although we have no quantitative measure of how successfully we have approached plug flow in the observation vessel, we have succeeded in at least uniformly filling the vessel with O_2 from the discharge, as substantiated by our visible observations and by the $O_2(^1\Sigma)$ concentration profiles shown in Figures 2-4. Measurements with a hot wire anemometer would help to establish the degree of flow speed uniformity.

At room temperature and 1 Torr, the diffusion coefficient for O_2 is ~ 150 cm^2 sec^{-1}. Under these conditions the average distance a molecule of O_2 will diffuse is ~ 25 cm. At linear flow speeds of 5 - 15 cm/sec, diffusion represents a significant deviation from the idealized method of extracting time from flow speed and distance measurements. Since diffusion occurs both

in the forward and backware direction, the net effect is to reduce concentration gradients and yield apparent species decay rates which are smaller than the true rates. We have not corrected for the effects of diffusion in the present experiment. Adding a buffer gas diluent should reduce the diffusion coefficient without significantly affecting quenching rates.

C. Kinetic Analysis

The differential rate equation governing the production and loss of $O_2(^1\Delta)$ is given as follows:

$$\frac{d[^1\Delta]}{dt} = - k_{\Delta 1}[^3\Sigma][^1\Delta] - 2\, k_p\, [^1\Delta]^2 - k_{HE}[^1\Delta] + k_{\Sigma 1}[^1\Sigma][^3\Sigma] + k_{\Sigma 2a}[^1\Sigma][^1\Delta] \qquad (13)$$

In Equation (13) the $O_2(^1\Delta)$ loss terms represent the rate of quenching of $O_2(^1\Delta)$ by ground state O_2, wall quenching, and energy pooling, while the positive terms reflect production of $O_2(^1\Delta)$ via quenching of $O_2(^1\Sigma)$ by $O_2(^3\Sigma)$ and by $O_2(^1\Delta)$.

The rate equation governing production and loss of $O_2(^1\Sigma)$ is given by:

$$\frac{d[^1\Sigma]}{dt} = - k_{\Sigma 1}[^3\Sigma][^1\Sigma] - k_{\Sigma 2}[^1\Delta][^1\Sigma] - k_x[X][^1\Sigma] - k'_{HE}[^1\Sigma] + k_p[^1\Delta]^2 \qquad (14)$$

with $k_{\Sigma 2} = k_{\Sigma 2a} + k_{\Sigma 2b}$.

The $O_2(^1\Sigma)$ loss terms in Equation (13) reflect quenching by $O_2(^3\Sigma)$, quenching by $O_2(^1\Delta)$ and quenching by trace impurities, i.e. H_2O, O_3, O etc. and wall quenching. The only production mechanism for $O_2(^1\Sigma)$ is energy pooling. Comparison of terms in Equations (13) and (14) reveal the assump-

tions that the first term in Equation (11) reflects quenching of $O_2(^1\Sigma)$ to $O_2(^1\Delta)$, while quenching by impurities leads to the ground state.

In the present system, $[^1\Delta]/[^3\Sigma] \lesssim 0.08$ and $[^1\Sigma]/[^3\Sigma] \lesssim 10^{-2}$, so that the last two terms in Equation (13) may be neglected unless $k_{\Sigma 1}$ and $k_{\Sigma 2a}$ are very large. Using the published rate constants for pooling and quenching by ground state O_2 (Table 1), it is easily shown that at 1 Torr total O_2 pressure, quenching of $O_2(^1\Delta)$ by ground state exceeds loss by pooling at $O_2(^1\Delta)$ fractions lower than 0.08. Thus at $O_2(^1\Delta)$ conversion fractions significantly lower than this value (i.e. < 0.005) we may write Equation (13) without serious loss of accuracy as:

$$\frac{d[^1\Delta]}{dt} = - k_{\Delta 1} [^3\Sigma][^1\Delta] = - k'_{\Delta 1} [^1\Delta] \qquad (15)$$

Equation (15) may be integrated, giving a pseudo-first order expression describing the decay of $O_2(^1\Delta)$:

$$[^1\Delta] = [^1\Delta]_o e^{-k'_{\Delta 1} t} \qquad (16)$$

As shown in Section B, an evaluation of the magnitude of the terms in Equation (14) reveals that the rate of heterogeneous quenching of $O_2(^1\Sigma)$ by the vessel wall is of the same order of magnitude as quenching by $O_2(^3\Sigma)$ at pressures below 1 Torr. Similarly, trace quantities of H_2O, O_3 and O are expected to be significant quenchers of $O_2(^1\Sigma)$ at densities of a few parts per million. Applying the steady state criterion to the evolution of $O_2(^1\Sigma)$ density, we obtain the following expression:

$$\frac{d[^1\Sigma]}{dt} = - k_{\Sigma 1}[^3\Sigma][^1\Sigma] - k_{\Sigma 2}[^1\Delta][^1\Sigma] - k_x[X][^1\Sigma] - k'_{HE}[^1\Sigma] + k_p [^1\Delta]^2 = 0 \qquad (17)$$

$$[^1\Sigma]_{ss} = \frac{k_p\,[^1\Delta]^2}{k_{\Sigma 1}[^3\Sigma] + k_{\Sigma 2}[^1\Delta] + k_x\,[X] + k'_{HE}} \tag{18}$$

If ground state O_2 is the dominant quenching source for $O_2(^1\Sigma)$, then

$$[^1\Sigma]_{ss} = \frac{k_p\,[^1\Delta]^2}{k_{\Sigma 1}[^3\Sigma]} \tag{19}$$

In the present experiments $[^1\Delta]/[^3\Sigma] \tilde{=} 0.1$ so that

$$\frac{[^1\Sigma]_{ss}}{[^1\Delta]_{ss}} = 0.1\,\frac{k_p}{k_{\Sigma 1}} = 0.05 \tag{20}$$

At 1 Torr total pressure, Equation (20) predicts steady state density of $O_2(^1\Sigma)$ of about 10^{14} cm^{-3}.

Rate Equation (14) may be solved exactly for $[^1\Sigma](t)$ in the limit where (16) is valid, i.e. where $[^1\Delta]/[^3\Sigma] \leq 0.005$. Substituting Equation (16) into Equation (14) we obtain a linear, nonhomogeneous differential equation.

$$\frac{d[^1\Sigma]}{dt} = -\,(k_{\Sigma 1}[^3\Sigma] + k_{\Sigma 2}[\Delta]_o e^{-k'_{\Delta 1}t} + k_x\,[X] + k'_{HE})[^1\Sigma] + k_p\,[^1\Delta]_o^2 e^{-2\,k'_{\Delta 1}t} \tag{21}$$

$$= -\,(k_Q + k_{\Sigma 2}[\Delta]_o e^{-k'_{\Delta 1}t})\,[^1\Sigma] + k_p[\Delta]_o^2 e^{-2\,k'_{\Delta 1}t} \tag{22}$$

$$k_Q = k_{\Sigma 1}[^3\Sigma] + k_x[X] + k'_{HE} \tag{23}$$

This equation may be solved by the method of undetermined coefficients:

$$[^1\Sigma](t) = \alpha \exp\left[-\left(k_Q - k_{\Sigma 2}[\Delta]_o e^{-k'_{\Delta 1}t}\right)\right]t + \frac{k_p[\Delta]_o^2 e^{-2k'_{\Delta 1}t}}{\left[k_Q + k_{\Sigma 2}[\Delta]_o e^{k'_{\Delta 1}t}\right] - 2k'_{\Delta 1}} \quad (24)$$

where α is an arbitrary constant. Using the initial condition, $[^1\Sigma](0) = 0$, we obtain:

$$[^1\Sigma](t) = \frac{k_p[\Delta]_o^2 e^{-2k'_{\Delta 1}t}}{\left[\left(k_Q + k_{\Sigma 2}[\Delta]_o e^{-k'_{\Delta 1}t}\right) - 2k'_{\Delta 1}\right.} \quad (25)$$

$$- \frac{k_p[\Delta]_o^2}{\left[\left(k_Q + k_{\Sigma 2}[\Delta]_o - 2k'_{\Delta 1}\right]\right.} \exp\left\{-\left(k_Q - k_{\Sigma 2}[\Delta]_o e^{-k'_{\Delta 1}t}\right)\right\}t$$

Equation (25) predicts that $O_2(^1\Sigma)$ density will build up to a maximum value with time constant determined by the total quenching rate of $O_2(^1\Sigma)$, then decay to zero with time constant $2k'_{\Delta 1}$. This analysis is similar to those given by O'Brien and Myers[33] and Heidner et al[35] but includes $[^1\Delta](t)$ as a quenching species.

The effect of quenching of $O_2(^1\Sigma)$ by $O_2(^1\Delta)$ is expressed in the time dependence of the denominator of the first term in Equation (25). If $k_{\Sigma 2}[\Delta]_o \cong k_Q$, the effective rate constant for decay of $O_2(^1\Sigma)$ would initially exceed $2k'_{\Delta 1}$, then approach $2k'_{\Delta 1}$ as $O_2(^1\Delta)$ decayed away.

Although not attempted in the present investigation, a trace of I_2 may be introduced into the system in order to enhance the pooling rate. Kinetics studies[34-36] pertaining to operation of the chemical oxygen-iodine laser have led to the elucidation of the following reaction sequence:

$$n\, O_2(^1\Delta) + I_2 \rightarrow n\, O_2(^3\Sigma) + 2I \quad (26)$$

$$I + O_2(^1\Delta) \xrightarrow{k_{27}} I^* + O_2(^3\Sigma) \quad (27)$$

$$I^* + O_2(^1\Delta) \xrightarrow{k_{28}} I + O_2(^1\Sigma) \qquad (28)$$

The rate constant for Reaction (28) is reported[35] to be 6 x 10^3 times greater than that for Reaction (1), and thus, any disadvantages attending the addition of iodine might be offset by the enhanced pooling rate.

In the COIL laser, energy pooling is a major detriment. Reaction (1) depletes $O_2(^1\Delta)$ between the generator and the laser, while Reaction (28) is a dominant quenching pathway once iodine is mixed into the flow. Under these conditions, a steady state develops described by

$$\frac{d[^1\Sigma]}{dt} = k_p[^1\Delta]^2 + k_{28}[^1\Delta]\,[I^*] - (k_Q + k_{\Sigma 2}[^1\Delta])[^1\Sigma] \qquad (29)$$

$$[^1\Sigma]_{ss} = \frac{[^1\Delta]}{(k_Q + k_{\Sigma 2}[^1\Delta])}\,(k_p[^1\Delta] + k_{28}[I^*]) \qquad (30)$$

Since the equilibrium between I^* and $O_2[^1\Delta]$ is established very rapidly:

and thus
$$[I^*] = K\,\frac{[I]}{[^3\Sigma]}\,[^1\Delta] \qquad (31)$$

$$[^1\Sigma]_{ss} = \frac{[^1\Delta]^2\,(k_p + k_{28}\,K[I]/[^3\Sigma]}{(k_Q + k_{\Sigma 2}[^1\Delta])} \qquad (32)$$

When I is not present in the mixture, Equation (32) of course reduces to Equation (18).

D. Results and Discussion

We have fit the data to the first order decay of $O_2(^1\Delta)$ and $O_2(^1\Sigma)$ predicted by Equations (16) and (25) for a variety of flow conditions. A representative decay plot for $O_2(^1\Delta)$ and $O_2(^1\Sigma)$ is shown in Figure 5. Within experimental uncertainty all such plots exhibited linearity, with the ratio of the slopes $m(^1\Sigma)/m(^1\Delta)$ approximately equal to 2 as predicted by Equation (25). The decay constants ($k'_{\Delta 1} = k_{\Delta 1}[^3\Sigma]$) derived from the slopes of these plots give values of $k_{\Delta 1}$ which fall into the range of values obtained by previous workers. These results suggest that $O_2(^1\Delta)$ is being quenched largely by $O_2(^3\Sigma)$ (see Table 1). Another important conclusion obtained from these results is that we are unable to observe the density maximum predicted by Equation (25). Not even at the highest linear flow speeds attempted (100 cm/sec) were we able to resolve the rise or maximum in the $O_2(^1\Sigma)$ population. This could be because the maximum occurred in the upstream portion of the apparatus beyond the viewing range of the PMT. A direct measurement of the $O_2(^1\Sigma)$ risetime would yield a time constant τ which reflected the total pseudo-first order rate constant for $O_2(^1\Sigma)$ destruction:

$$\tau = [k_Q + k_{\Sigma 1}{}^{\Delta}{}_o e^{-k'_{\Delta 1} t}]^{-1} \qquad (33)$$

In order to assess the magnitude the rate constant for quenching of $O_2(^1\Sigma)$ by $O_2(^1\Delta)$ it was necessary to establish the magnitude of quenching by other species, especially those whose concentration changes with time (e.g. O_3, O). In the absence of all quenchers except ground state O_2, Equation (19) predicts that the steady state ratio of $O_2(^1\Sigma)$ to $O_2(^1\Delta)$ is given by

$$\frac{[^1\Sigma]_{ss}}{[^1\Delta]} = \frac{k_p[^1\Delta]}{k_{\Sigma 1}[^3\Sigma]} \tag{34}$$

The r.h.s. of Equation (34) thus determines the upper limit of the $O_2(^1\Sigma)$ to $O_2(^1\Delta)$ ratio. A quenching species whose density was time independent would suppress $[^1\Sigma]_{ss}$ but would not affect the rate constant describing its rate of decay in the observation vessel at long times. This rate of decay is determined by $k_{\Delta 1}$. A quenching species whose density decreased with time would similarly suppress $[^1\Sigma]$, but the magnitude of the effect would decrease with time.

If $k_{\Sigma 2} \sim k_{\Sigma 1}$, the resulting plot of $[^1\Sigma]$ vs. time would be expected to exhibit a monotonic decay at $t >> t_m$ where t_m is the time at which $[^1\Sigma]$ reaches a maximum. In this regime the decay constant describing $O_2(^1\Sigma)$ disappearance would be greater than $2k'_{\Delta 1}$, but would approach this value as the density of the quencher decreased with time.

Since $[O_2] \cong [^3\Sigma] + [^1\Delta]$ we can write as Equation (18)

$$[^1\Sigma]_{ss} = \frac{k_p[^1\Delta]^2}{(k_{2\Sigma} - k_{1\Sigma})\,[^1\Delta] + k_{1\Sigma}[O_2] + k_x[X] + k'_{HE}} \tag{35}$$

which can be rearranged to

$$\frac{[^1\Delta]}{[^1\Sigma]_{ss}} = k_i + k_s\,[^1\Delta]^{-1} \tag{36}$$

where $k_i = (k_{2\Sigma} - k_{1\Sigma})/k_p$ and $k_s = \dfrac{k_{1\Sigma}\,[O_2] + k_x\,[X] + k'_{HE}}{k_p}$

A plot of the ratio $[^1\Delta]/[^1\Sigma]$ vs. $[^1\Delta]^{-1}$ is expected to yield a straight line with slope k_s and intercept k_i. Thus from one graph we may extract the magnitude of quenching of $O_2(^1\Sigma)$ by the wall and by species other than $O_2(^3\Sigma)$

from the slope and $k_{\Sigma 2}$ from the intercept. Such plots obtained under several sets of conditions are shown in Figures 6-8. As these figures show there is some noise in the plotted data. It is suspected that the major source of this noise is the distortion caused by the nonuniform glass surface of the Pyrex observation vessel. Visually, the vessel surface is slightly rippled and is far from good optical quality. Furthermore the vessel walls become thicker toward the ends, and some attenuation at 1.27 μm was noted at these positions. For this reasons data were taken but not reported at positions where attenuation was notice-able. The experimentally determined values of k_i are listed in Table 3.

Values of k_f, k_s and their uncertainty limits were evaluated using a standard linear regression statistics package (IMSL). The uncertainties represent one standard deviation at the (± 68%) confidence level. Values of $k_{\Sigma 2}$ calculated from k_f using Equation (36) are given in Table 3. The magnitude of the standard errors associated with the independent measurements of $k_{\Sigma 2}$ are relatively large, however averaging all independent determinations, we obtain $k_{\Sigma 2} = 6.5 \pm 6.1 \times 10^{-16}$ cm^3 molec^{-1} sec^{-1}.

Within the statistical uncertainty of our measurements, we conclude that the rate constant $k_{\Sigma 2}$ for quenching of $O_2(^1\Sigma)$ by $O_2(^1\Delta)$ is comparable to $k_{\Sigma 1}$, the rate constant for quenching by ground state oxygen. Possible sources of error in the estimation of $k_{\Sigma 2}$ include:

1. Uncertainty in $O_2(^1\Delta)$ and $O_2(^1\Sigma)$ density measurements arising from optical variations in the viewing vessel.
2. Systematic errors due to quenching of $O_2(^1\Sigma)$ by residual O_3 or oxygen atoms.
3. Errors in interpretation due to axial diffusion within the measurement vessel.

Our experimentally determined values of k_s obtained via Equation (36) yield values of $k_{\Sigma 1}$ which agree well within previously determined values of $k_{\Sigma 1}$, which suggests that quenching of $O_2(^1\Sigma)$ by O_3 and O have been effectively eliminated and that for $P \geq 4$ Torr, heterogeneous quenching is unimportant.

The evaluation of any error introduced by axial diffusion of components within the vessel is difficult. However, since the measured values of the rate constants for quenching of $O_2(^1\Sigma)$ and $O_2(^1\Delta)$ by ground state oxygen (i.e. $k_{\Delta 1}$ and $k_{\Sigma 1}$) are in the range of previous determinations, it appears that the effect is small. The fact that diffusion distances in 1 sec at 1 Torr do not greatly exceed distances traveled by the flow, would tend to support this conclusion, however further investigation is needed in Phase II.

After evaluating these sources of error, we have concluded that the variable viewing efficiency through the glass vessel is the major source and that the resulting errors in density measurement, though systematic in fact, appear random, at least at axial positions away from the ends of the vessel.

In the absence of heterogeneous quenching and quenching by trace impurities,

$$k_s^{\,o} = \frac{k_{\Sigma 1}[O_2]}{k_p} \tag{37}$$

A measured value of k_s greater than this lower limit indicates that $O_2(^1\Sigma)$ is probably being quenched by some pathway other than quenching by ground state oxygen. As shown in Table 3, the derived values of $k_{\Sigma 1}$ are somewhat higher than the literature value at $P < 1$ Torr, but at $P > 4$ Torr, the agreement is very good.

We believe that this is the first singlet oxygen experiment to achieve

$O_2(^1\Sigma)$ densities limited only by homogeneous quenching by ground state O_2. The number densities of $O_2(^1\Sigma)$ reported here ($> 10^{13}$ cm^{-3}) appear to be the highest yet achieved. Other investigations have been conducted in small diameter flow systems where wall quenching was the dominant source of $O_2(^1\Sigma)$ deactivation.

E. Summary

We have constructed and successfully demonstrated a discharge-flow apparatus for $O_2(^1\Delta)$ and $O_2(^1\Sigma)$ kinetics studies. Some important results obtained include:

1) Verification of the rate constant for quenching of $O_2(^1\Delta)$ by ground state oxygen.

2) Attainment of $O_2(^1\Sigma)$ concentrations limited predominantly by the rate of quenching of $O_2(^1\Sigma)$ by ground state O_2. We believe that this is the first discharge-flow experiment to produce $O_2(^1\Sigma)$ under conditions where wall quenching or quenching by impurities were not the dominant factors limiting the steady state density of $O_2(^1\Sigma)$.

3) Estimation of $k_{\Sigma 2}$, the rate constant for quenching of $O_2(^1\Sigma)$ by $O_2(^1\Delta)$. Although the value obtained for $k_{\Sigma 2}$ is somewhat uncertain due to noisy data, its magnitude ($6.5 \pm 6.1 \times 10^{-16}$ cm^3 $molec^{-1}$ sec^{-1}) is not extremely large compared to $k_{\Sigma 1}$, the rate constant for quenching by ground state O_2. We find these preliminary results very encouraging as they pertain to the feasibility of the Red SOX laser.

References

1. W. E. McDermott, N. R. Pchelkin, D. J. Benard, and R. R. Bousek, Appl. Phys. Lett. 32, 469 (1978)

2. D. J. Benard, W. E. McDermott, N. R. Pchelkin, and R. R. Bousek, Appl. Phys. Lett. 34, 40 (1979)

3. K. Watanabe, S. Kashiwabara, K. Sawai, S. Toshima, and R. Fujimoto, J. Appl. Phys. 54, 1228 (1983)

4. A. K. MacKnight, R. D. Franklin and R. L. Kerber, Electronic Transition Lasers II, L. E. Wilson, S. N. Suchard, and J. I. Steinfeld, Ed., MIT Press, Cambridge, MA, p. 305 (1976)

5. R. L. Kerber, A. K. MacKnight, and R. D. Franklin, Appl. Opt. 17, 3276 (1978)

6. G. A. Fisk and G. N. Hays, J. Chem. Phys. 77, 4965 (1982)

7. R. G. Derwent and B. A. Thrush, Trans. Faraday Soc. 67, 2036 (1971)

8. K. H. Becker, W. Groth and V. Schurath, Chem. Phys. Lett. 8, 259 (1971)

9. I. D. Clark and R. P. Wayne, Chem. Phys. Lett. 3, 405 (1969)

10. T. G. Slanger and G. Black, J. Chem. Phys. 70, 3434 (1979)

11. I. D. Clark, I. T. N. Jones and R. P. Wayne, Proc. Roy. Soc., London Ser. A 317, 407 (1970)

12. F. D. Findley and D. R. Snelling, J. Chem. Phys 54, 2750 (1971)

13. R. G. Aviles, D. F. Muller and P. L. Houston, Appl. Phys. Lett. 37, 358 (1980)

14. P. Borrell, P. M. Borrell and M. D. Pedley, Chem. Phys. Lett. 51, 300 (1977)

15. A. Leiss, V. Schurath, K. H. Becker and E. H. Fink, J. Photochem. 8, 211 (1978)

16. W. C. Eisenberg, A. Snelson, R. Butler and K. Taylor, J. Photochem. 25, 439 (1984)

17. R. P. Steer, R. A. Ackerman and J. N. Pitts, Jr., J. Chem. Phys. 51, 843 (1969)

18. K. Tachibana and A. V. Phelps, J. Chem. Phys. 75, 3315 (1981)

19. I. D. Clark and R. P. Wayne, Proc. Roy. Soc. Lond. A. 314, 111 (1969)

20. S. A. Lawton and A. V. Phelps, J. Chem. Phys. 69, 1055 (1978)

21. J. F. Noxon, J. Chem. Phys. 52, 1852 (1970)

22. S. V. Filseth, A. Zia and K. H. Welge, J. Chem. Phys. 52, 5502 (1970)

23. T. P. J. Izod and R. P. Wayne, Proc. Roy. Soc. A. 308, 81 (1968)

24. J. P. S. Chatha, P. K. Arora, SMT Nalini Raja, P. B. Kulkarni and K. G. Vohra, Int. J. Chem. Kin. 11, 175 (1979)

25. S. A. Lawton, S. E. Novick, H. P. Broida and A. V. Phelps, J. Chem. Phys. 66, 1381 (1977)

26. R. G. O. Thomas and B. A. Thrush, J. Chem. Soc. Farad, Trans. 2, 71, 664 (1975)

27. F. Stuhl and K. H. Welge, Can. J. Chem. 47, 1870 (1969)

28. K. Kear and E. W. Abrahamson, J. Photochem. 3, 409 (1974)

29. P. Borrell, P. M. Borrell, D. S. Richards and R. B. Boodaghians, J. Photochem. 25, 339 (1984)

30. L. Robbin Martin, R. B. Cohen and J. F. Schatz, Chem. Phys. Lett. 41, 394 (1976)

31. M. Yaron and A. Von Engel, Chem. Phys. Lett. 33, 316 (1975)

32. G. Black and T. G. Slanger, J. Chem. Phys. 74, 6517 (1981)

33. R. J. O'Brien and G. H. Myers, J. Chem. Phys. 53, 3832 (1970)

34. H. V. Lilenfeld, Oxygen Iodine Laser Kinetics, U. S. Air Force Report AFWL-TR-83-01 (1983)

35. R. F. Heidner III, C. E. Gardner, T. M. El-Sayed, G. I. Segal, and J. V. V. Kasper, J. Chem. Phys. 74, 5618 (1981)

36. R. F. Heidner III, J. Photochem. 25, 449 (1984)

Table 1. Bimolecular rate constants for reactions involving $O_2(^1\Delta)$ and $O_2(^1\Sigma)$. The primary reference containing the "preferred" rate constant value from Reference 40 is listed first.

Reaction	Rate Constant $(cm^3\ molec^{-1}\ sec^{-1})$]	References
$2\ O_2(^1\Delta) \xrightarrow{k_p} O_2(^1\Sigma) + O_2(^3\Sigma)$	$2.03 \pm 0.50 \times 10^{-17}$	6,7
$O_2(^1\Delta) + NO_2 \rightarrow O_2(^3\Sigma) + NO_2$	$5.0 \pm 1.0 \times 1.0^{-18}$	8
$O_2(^1\Sigma) + NO_2 \rightarrow O_2(^1\Delta, ^3\Sigma) + NO_2$	$2.5 \pm 0.5 \times 10^{-14}$	8
$O_2(^1\Delta) + O \rightarrow O_2(^3\Sigma) + O$	$\leq 1.3 \times 10^{-16}$	9
$O_2(^1\Sigma) + O \rightarrow O_2(^1\Delta, ^3\Sigma) + O$	$8.0 \pm 2.0 \times 10^{-14}$	10
$O_2(^1\Delta) + O_3 \rightarrow 2\ O_2(^3\Sigma) + O$	$3.5 \pm 0.5 \times 10^{-15}$	11,12
$O_2(^1\Sigma) + O_3 \rightarrow 2\ O_2(^3\Sigma) + O$	$2.2 \pm 0.2 \times 10^{-11}$	10
$O_2(^1\Sigma) + H_2O \rightarrow O_2(^1\Delta, ^3\Sigma) + O$	$6.71 \pm 0.53 \times 10^{-12}$	13
$O_2(^1\Delta) + O_2(^3\Sigma) \rightarrow 2\ O_2(^3\Sigma)$	$1.56 \pm 0.05 \times 10^{-18}$	14-19
$O_2(^1\Sigma) + O_2(^3\Sigma) \rightarrow O_2(^1\Delta) + O_2(^1\Delta, ^3\Sigma)$	$4.0 \pm 0.4 \times 10^{-17}$	30,8,20-29
$O_3 + O \rightarrow 2O_2$	6.2×10^{-15}	31

Table 2. Contributions to the heterogeneous rate constant for quenching of $O_2(^1\Sigma)$ and $O_2(^1\Delta)$. Values were obtained using $\gamma(O_2\,^1\Delta) = 10^{-5}$, $\gamma(O_2\,^1\Sigma) = 2.5 \times 10^{-3}$, and $D_o = 144$ Torr cm^2 sec^{-1}.

P(Torr)	$\frac{r^2 P}{8 D_o}$ (sec)	$\frac{2r}{\gamma\bar{u}}$ (sec)		K_{HE} (sec^{-1})	
		$O_2(^1\Delta)$	$O_2(^1\Sigma)$	$O_2(^1\Delta)$	$O_2(^1\Sigma)$
0.1	0.08			7.4×10^{-3}	1.61
0.5	0.4			7.4×10^{-3}	0.94
1.0	0.8	135	0.54	7.4×10^{-3}	0.75
5.0	4			7.2×10^{-3}	0.22
10.0	8			7.0×10^{-3}	0.12

Table 3. Rate constants derived from experimental data (see Figures 6-8). Values for $k_{\Sigma 1}$ and $k_{\Sigma 2}$ were calculated using Equation (33). Units for $k_{\Sigma 1}$ and $k_{\Sigma 2}$ are cm^3 $molec^{-1}$ sec^{-1}.

Expt	Figure	k_s ($\frac{molecule}{cm^3}$)	k_1	$k_{\Sigma 1}$	$k_{\Sigma 2}$
1	6	$4.5 \pm 0.9 \times 10^{17}$	54 ± 47	$2.6 \pm 0.5 \times 10^{-16}$	$1.1 \pm 1.0 \times 10^{-15}$
2	7	$8.3 \pm 1.0 \times 10^{17}$	0 ± 43	$3.7 \pm 0.4 \times 10^{-16}$	$4 \pm 86 \times 10^{-17}$
3	8	$2.7 \pm 0.2 \times 10^{17}$	112 ± 101	$4.0 \pm 0.3 \times 10^{-17}$	$2.2 \pm 2.0 \times 10^{-15}$
		Variance-weighted Average		$4.3 \pm 0.3 \times 10^{-17}$	0.065 ± 0.061

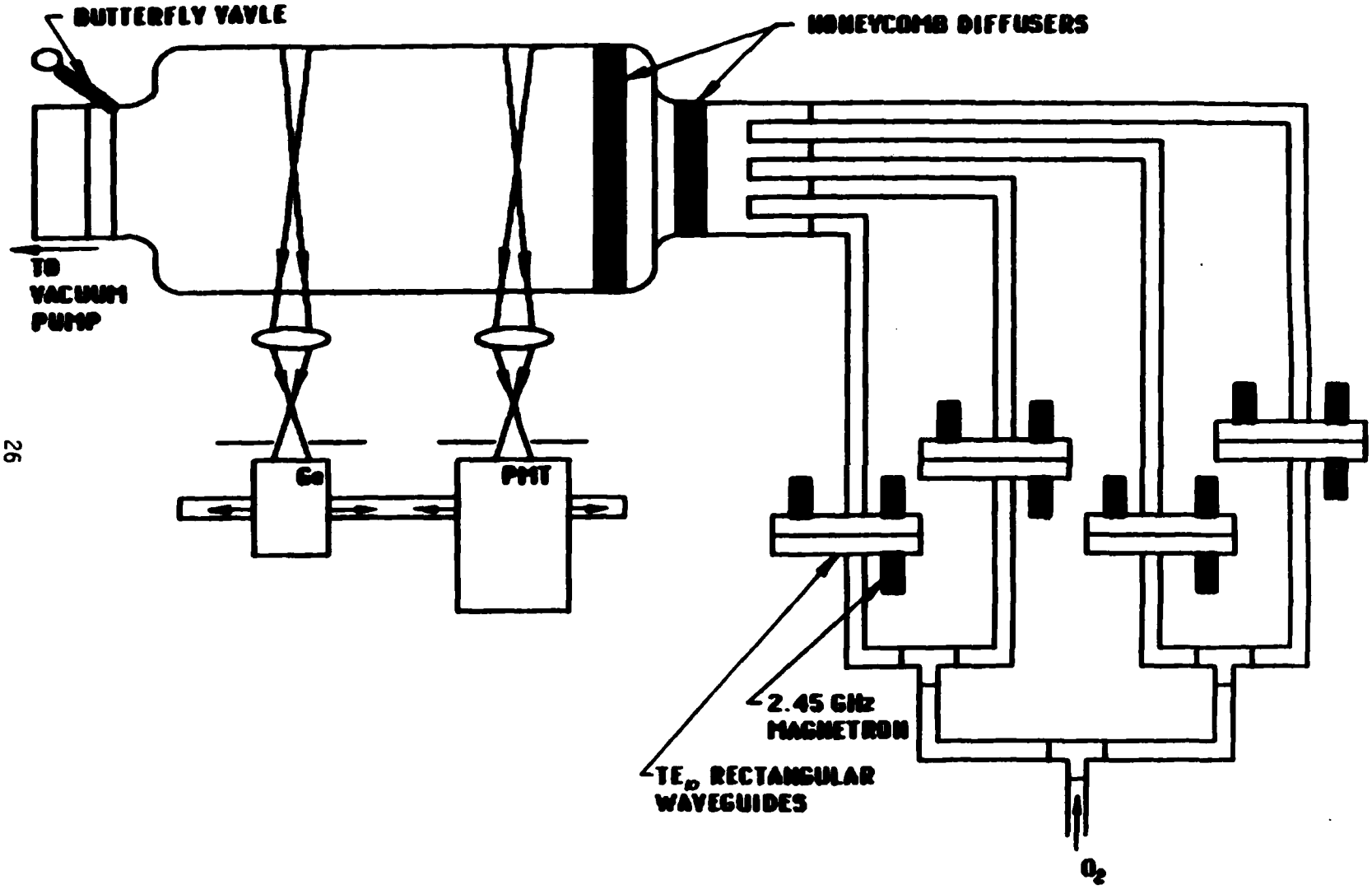

Figure 1. Schematic diagram of 60 cm diameter discharge-flow apparatus for $O_2(^1\Sigma)$ measurements.

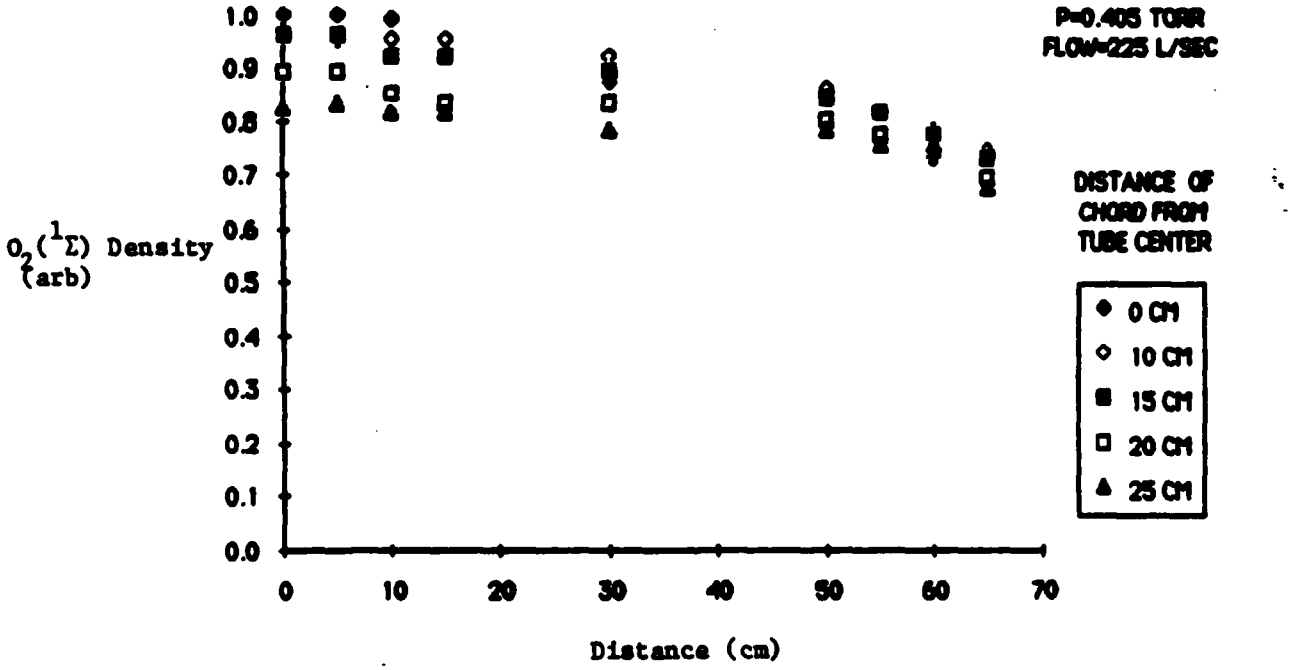

Figure 2. Relative $O_2(^1\Sigma)$ density measured at various distances from tube axis. Plotted on the horizontal axis is distance in the direction of the flow axis.

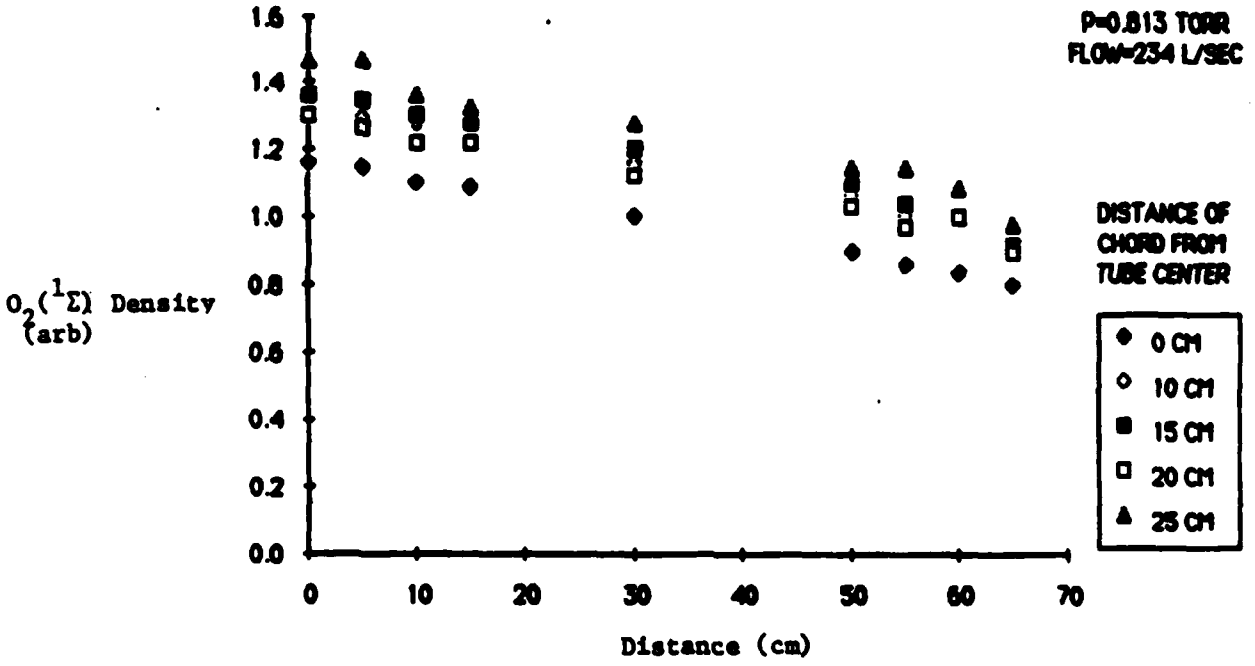
P=0.813 TORR
FLOW=234 L/SEC
DISTANCE OF CHORD FROM TUBE CENTER
0 CM
10 CM
15 CM
20 CM
25 CM
$O_2(^1\Sigma)$ Density (arb)
1.6
1.4
1.2
1.0
0.8
0.6
0.4
0.2
0.0
0
10
20
30
40
50
60
70
Distance (cm)

Figure 3.

28

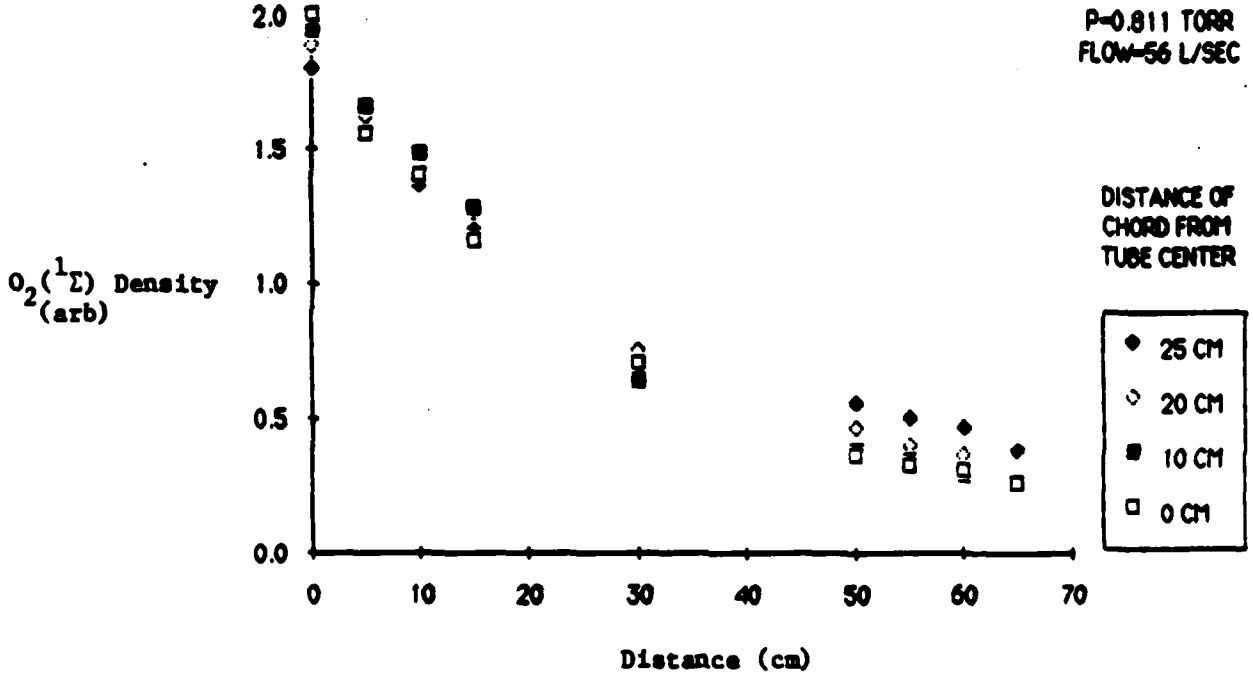
P=0.811 TORR
FLOW=56 L/SEC
DISTANCE OF CHORD FROM TUBE CENTER
25 CM
20 CM
10 CM
0 CM
$O_2(^1\Sigma)$ Density (arb)
2.0
1.5
1.0
0.5
0.0
0
10
20
30
40
50
60
70
Distance (cm)

Figure 4.

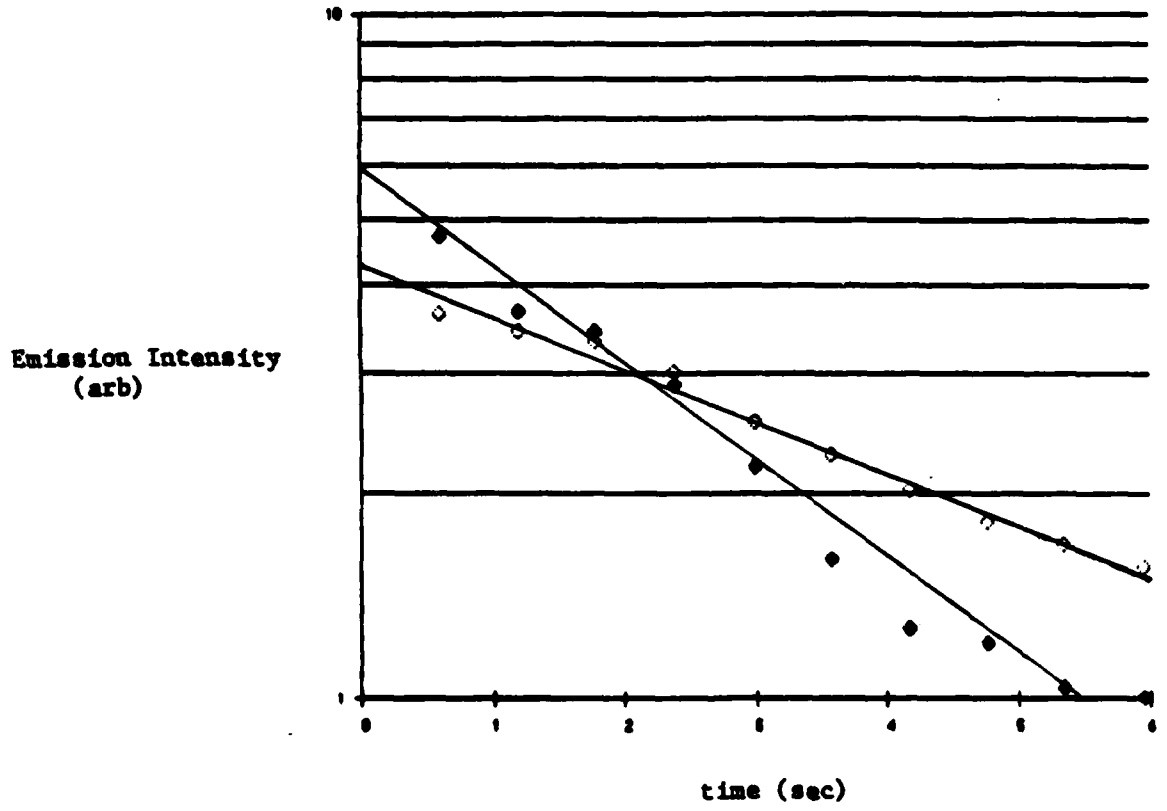

Figure 5. Time dependence of emission signal from $O_2(^1\Delta)$ (open diamonds) and $O_2(^1\Sigma)$ (filled diamonds).

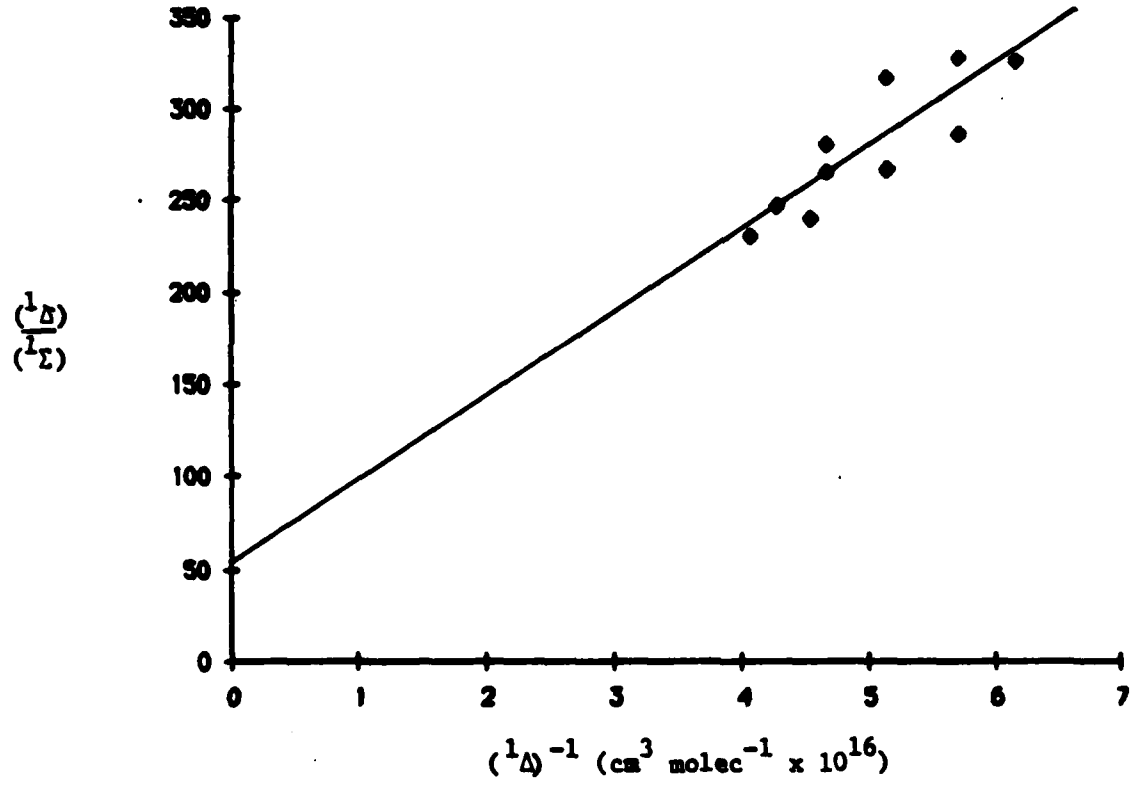

Figure 6. Determination of k_2 and k_1. Total pressure = 1.1 Torr; flow speed = 12.7 cm sec^{-1}.

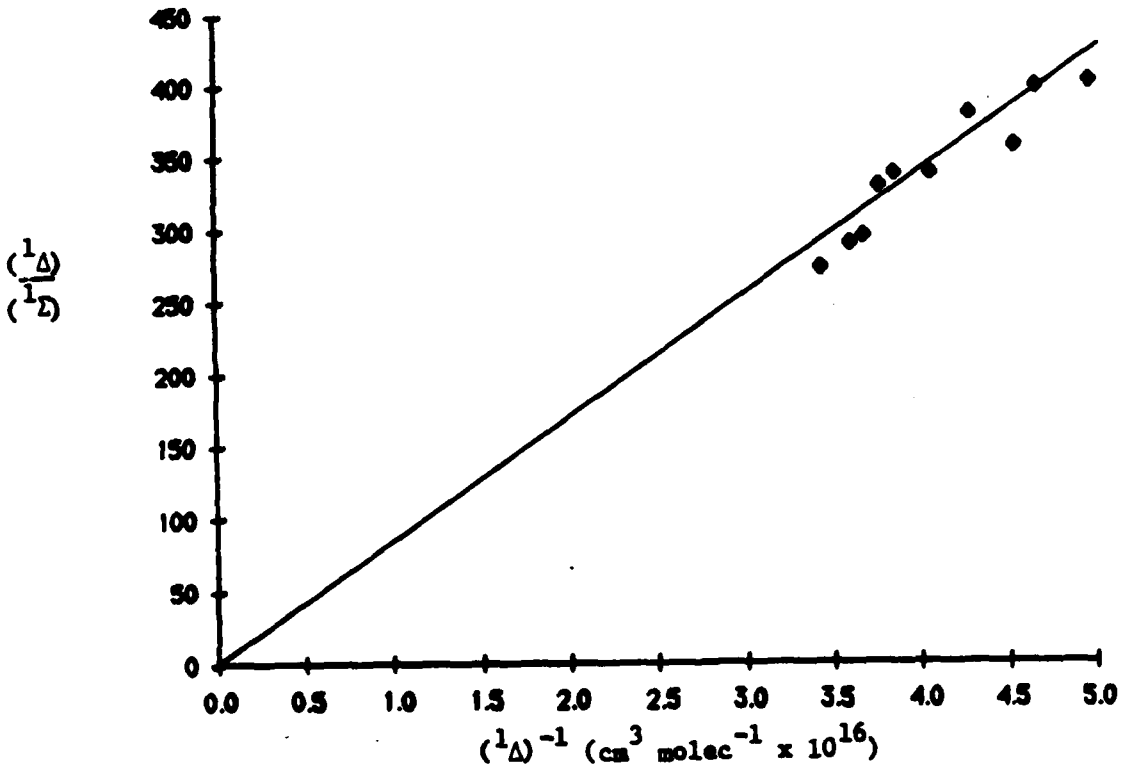

Figure 7. Total pressure = 1.4 Torr.
Flow speed = 15.9 cm sec^{-1}.

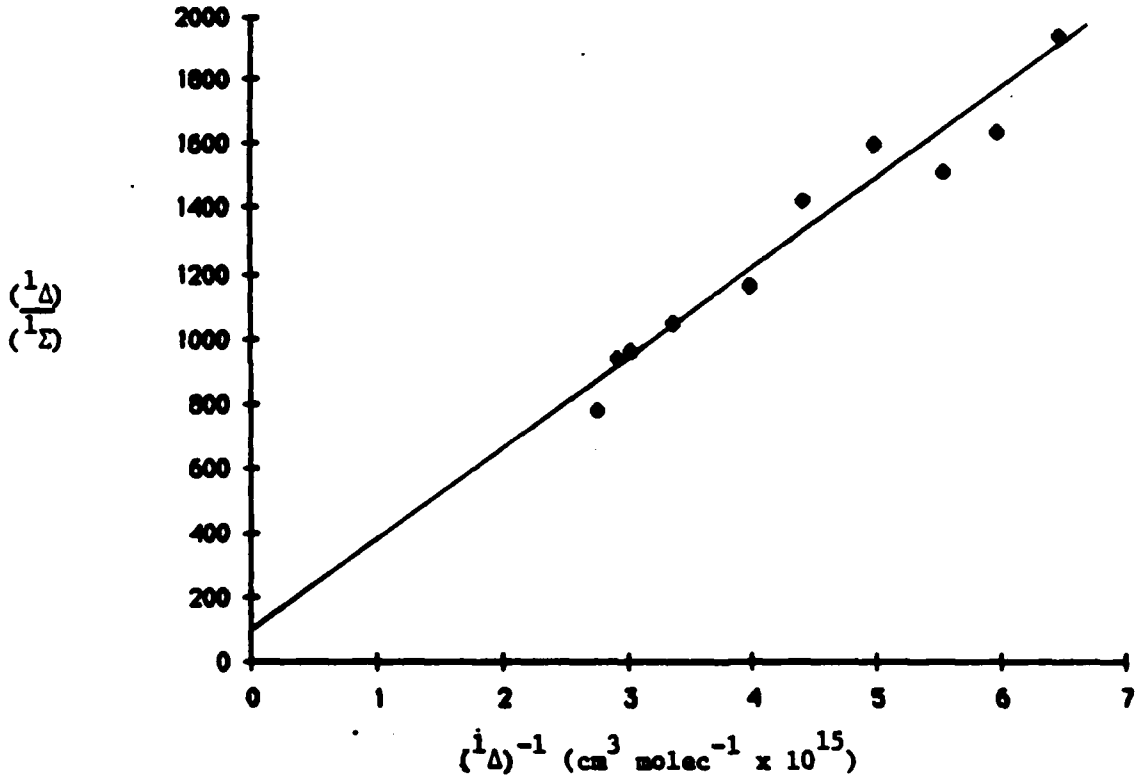

Figure 8. Total pressure = 4.2 Torr; flow speed = 8.4 cm sec^{-1}.

END

12-86

DTIC